TEKTONIKA

Supporting Information

for

Signatures of fluid-rock interactions in shallow parts of the San Andreas and San Gabriel Faults, southern California

James P. Evans[1], Kaitlyn A. Crouch[1,2], Caroline Studnicky[1,3], Sharon Bone[4], Nicholas Edwards[4], Samuel M. Webb[4]

[1]Department of Geosciences, Utah State University, Logan, UT 84322-4505

[2] now at Department of Geosciences, University of Wisconsin, Lewis G. Weeks Hall, 1215 West Dayton Street, Madison, WI 53706-1692

[3]now at: Chevron North America Exploration and Production, 6301 Deauville Boulevard Midland, TX 79706, U.S.A.

[4]Stanford Synchrotron Radiation Lightsource, SLAC National Accelerator Laboratory 2575 Sand Hill Road, MS 69 Menlo Park, CA 94025

File SI-1: Synchrotron methods and conditions

We examined the elemental distribution of rocks on three beamlines at the Stanford Synchrotron Radiation Laboratory (SSRL). The SPEAR (Stanford Positron Electron Accelerating Ring) storage ring operates at 500 mA beam current at 3.0 GeV, topped off every 5 minutes. For the thin-section samples, we collected data for XRF-maps on elements from sulfur to arsenic on beamlines 2-3, 6-2, and 10-2. Details of analysis conditions are in Table A1.

The SSRL beamline 2-3 enables the highest resolution mapping. On beamlines 2-3, we use a Si (111) double crystal monochromator for incident X-ray energy selection. The fluorescent lines of the elements are measured in an open-air hutch using a single-channel silicon drift Hitachi Vortex detector coupled to a Quantum Detectors Xspress3 multi-channel analyzer. Standard 2.7 x 4.6 cm polished thin sections were mounted on a rotating base at 45° to the incident X-ray beam, and 2 or 5 mm regions were rastered in the microbeam. At the same time, data were collected continuously during stage motion.

We examined 5 x 7.5 cm thin sections for large-scale XRF imaging on beamline 10-2, now 7-2. Thin sections are mounted on a flat plate and raster scanned at 45° relative to the incident X-ray beam. We use the SRS-XRF method with a Si (111) double crystal monochromator to select the incident energy. The fluorescent X-rays are measured with a four-element Hitachi Vortex ME4 silicon drift detector coupled to a Quantum Detectors Xspress3 multi-channel analyzer system for elemental XRF mapping in an open hutch.

On beamline 6-2 (see Edwards et al., 2018), we examined an ~80 cm long portion of drill core from the San Andreas Fault (Figure 4). Beamline 6-2 uses a continuous rapid-scan system with a sample area of up to 1000×600 mm, with 25–100 μm resolution provided by pinhole apertures. The fluorescence X-rays are measured with a four-element Hitachi Vortex ME4 silicon drift detector coupled to a Quantum Detectors Xspress3 multi-channel analyzer system for elemental XRF mapping.

The elemental maps were produced with SMAK (Webb, 2011). Most maps use a yellow-orange-red color ramp to indicate the element concentrations, measured in counts/second. The only option for the tricolor maps are red-green-blue.

Table SI-1: Summary of the XRF mapping conditions.

Sample	beamline	spot size (μm)	dwell time (ms)	Energy (eV)	Point range (x,y) and total time (sec)
SGF 51-1	10-2	25	25	8000	569 x 134; 4837
SGF 71-1	10-2	25	25	12500	793 x 684; 16202
SGF 71-1	10-2	25	25	12500	739 x 538; 11328
SGF 65A	10-2	10, 25, 50,75	25	12500	1501 x 367; 14937
SGF 65A	2-3	2, 5	25	7200	281x 601; 5367
SGF 96.1	10-2	25	25	12500	946 x 234; 6154
SGF 96.1	10-2	5	25	12500	1017 x 456; 12808
SGF 96-1	2-3	1.5	25	7200	1152 x 211; 7702
LE 4-130	2-3	2	25	7200	17092s
LE 6-134	10-2	25	25	13000	4336
LE 6-134	2-3	4, 5	25	7200	1865
LE 2-355	2-3	15	25	7200	846x139, 3567
LE 6-433	10-2	50	15	13000	1709 x 613; 18848
LE 6-433	2-3	15	10	7500	646 x 25725 4184
SAF LE core	6-2	25,50	10	11000	7754,10047;8541,12041
SAF core E	6-2	50	20	11000	12022

File SI-2: Quantification of elemental concentrations at grain scales

Sample 6-134.7 (Figure 17) allows quantifying and calibrating elemental concentrations between whole-rock data and the XRF maps to determine the microscale heterogeneity of elemental compositions in these rocks. Studnicky (2021) examined 12 San Andreas Fault samples with electron microprobe energy dispersive spectrometry (EDS) to determine the elemental concentrations in small areas of the samples. For sample 6-134.7, she examined 12 sites across the sample (Figure B1) for their major element compositions.

To make direct comparisons and analyses, we use standard whole–rock geochemical data (Table B1) expressed in weight percent oxides from 2-3 g aliquots and convert element-only concentrations in the EDS data (Table B2) to equivalent oxide values. To do this, we: 1) determine equivalent oxide values of the whole-rock data free of LOI, C, and O, 2) correct the data to express the iron values as total iron, FeO, and 3) convert the element analyses of the EDS data to oxide equivalents. We convert the iron weight percentage data in the whole rock analyses to convert from Fe_2O_3 to FeO (J. W. Shervais, pers. comm.) by determining a common conversion factor for all of the data:

Normalize factor data to 100% = (100-FeO*)/(Sum-Fe_2O_3*)

Where FeO*=Fe_2O_3* x 0.899

The 0.899 value is the conversion factor between the molecular weights of FeO and Fe_2O_3.

The whole rock data are recalculated and normalized to a volatile-free basis (Table B1) by subtracting the volatile components from the total analyses and recomputing the percentages.

Table SI-2:

Whole rock geochemical data for 6-134.7 as % oxide

SiO_2	Al_2O_3	Fe_2O_3	CaO	MgO	Na_2O	K_2O	Cr_2O_3	TiO_2	MnO	P_2O_5	SrO	BaO	LOI	Total
57.9	15.8	5.53	5.74	2.12	3.52	2.57	0	0.83	0.1	0.21	0.05	0.06	5.04	99.4
Norm Factor														
1.01														
SiO_2	Al_2O_3	FeO*	CaO	MgO	Na_2O	K_2O	Cr_2O_3	TiO_2	MnO	P_2O_5	SrO	BaO	LOI	total
58.24	15.84	4.98	5.77	2.13	3.54	2.59	0.00	0.83	0.10	0.21	0.05	0.06	5.04	99.39
Normalize Volatile-free														
1.05														
61.35	16.69	5.24	6.08	2.25	3.73P	2.72	0.00	0.88	0.11	0.22	0.05	0.06		99.39

The EDS data are converted into percentages of the elemental oxides akin to how the whole-rock data are determined so that we can compare like quantities. The EDS data provide values of oxygen and carbon, where the oxygen is a calculated value from the microprobe data reduction method, and the carbon is primarily due to carbon coating on the sample (Table B2). We renormalize the EDS data for only the major cations (Table B3) to determine a volatile free FeO analysis. We then convert the % Fe to an FeO value of the by:

(Oxide molecular weight of Fe x elemental weight of Fe)
the atomic weight of Fe

Which for iron becomes

(71.84 x elemental value of Fe in data)/55.84

= 1.28 x elemental value of Fe (Table B3).

Table SI-3: EDS data Sample 6-134.7

point	O	Si	C	Al	Fe	Na	Ca	Mg	Ti	K	Mn	Cl
2	42.7	18.3	16.8	7	6.1	2.6	2.5	2	1	0.8	0.2	0.2
3	42.7	18.6	15.2	6.2	7.9	1.4	3.2	2.4	1.2	0.8	0.2	
4	45.4	24.1	13.2	7.8	0.7	1.5	3.2	0.2	0.1	3.4		0.1
5	44.2	17.9	16.3	6.7	5	1.5	3.2	1.7	0.7	0.6	0.2	0.1
6	48.3	17	13.5	7.4	8	2.1	2	3.3	1	1.2	0.2	0.1
7	42.4	21.3	18.5	5.7	3	1.1	2.5	0.6	0.3	1.8		0.3
8	43.8	22.7	18.1	5.8	1.2	1.2	3.2	0.4	0.2	0.6		0.3
9	42.1	17.5	17.4	6.7	6.7	2.3	3	1.8	1.2	0.9	0.1	0.2
10	39.5	16.5	15.9	6.1	9.4	1.6	2.6	1.5	1.2	2.5	0.1	0.1
11	41.9	20	16.2	7	5.6	1.1	1.2	1.7	0.4	4.3	0.1	0.2
12	42.5	23.8	14.9	6.4	3.1	1.1	1.2	0.7	0.7	5.5	0.4	0.2
13		41.4	19.6	7.3	4.1	3.5	1.9	1	0.5	1.3		0.2
avg	43.23	21.59	16.30	6.68	5.07	1.75	2.48	1.44	0.71	1.98	0.19	0.18
sd	2.14	6.48	1.85	0.63	2.62	0.71	0.72	0.87	0.39	1.55	0.09	0.07
median	42.7	19.3	16.3	6.7	5.3	1.5	2.55	1.6	0.7	1.25	0.2	0.2

We use this to calculate the total iron concentrations at the 12 sites. The whole-rock value of 5.24% iron (Table B1) averages the iron value for a given aliquot. The sample map (Figure B1) shows that FeO varies from 1.04% in the host rock to 12% on the narrow slip surfaces. Since we treated all XRF maps the same regarding color ramps and scales, we also show that the darkest regions on the Fe maps represent Fe values > 8% for the samples analyzed.

Table SI-4: EDS data for Fe, Sample 6-134.7

Point	% FeO volatile free	% FeO Total Fe	enrichment relative to whole rock value
2	7.33	9.43	1.80
3	9.34	12.01	2.29
4	0.81	1.04	0.20
5	6.12	7.87	1.50
6	8.84	11.37	2.17
7	3.81	4.90	0.94
8	1.52	1.95	0.37
9	8.14	10.47	2.00
10	11.60	14.92	2.85
11	6.72	8.65	1.65
12	3.63	4.67	0.89
13	5.09	6.54	1.25

Supplemental Figure 1.

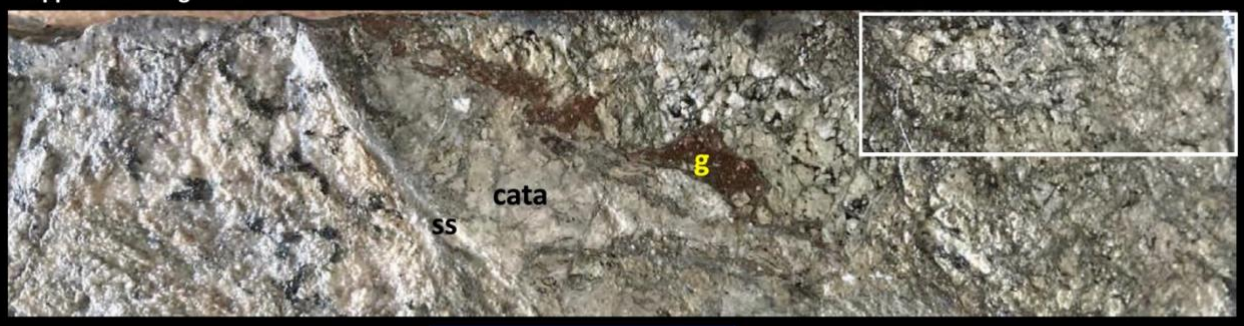

5 cm

Supplemental Figure 1A.

0	Fe	7100
0	Mn	1700
0	Ca	5000
0	Ti	3500
0	K	1800
0	Cr	400

San Andreas core zoomed in area

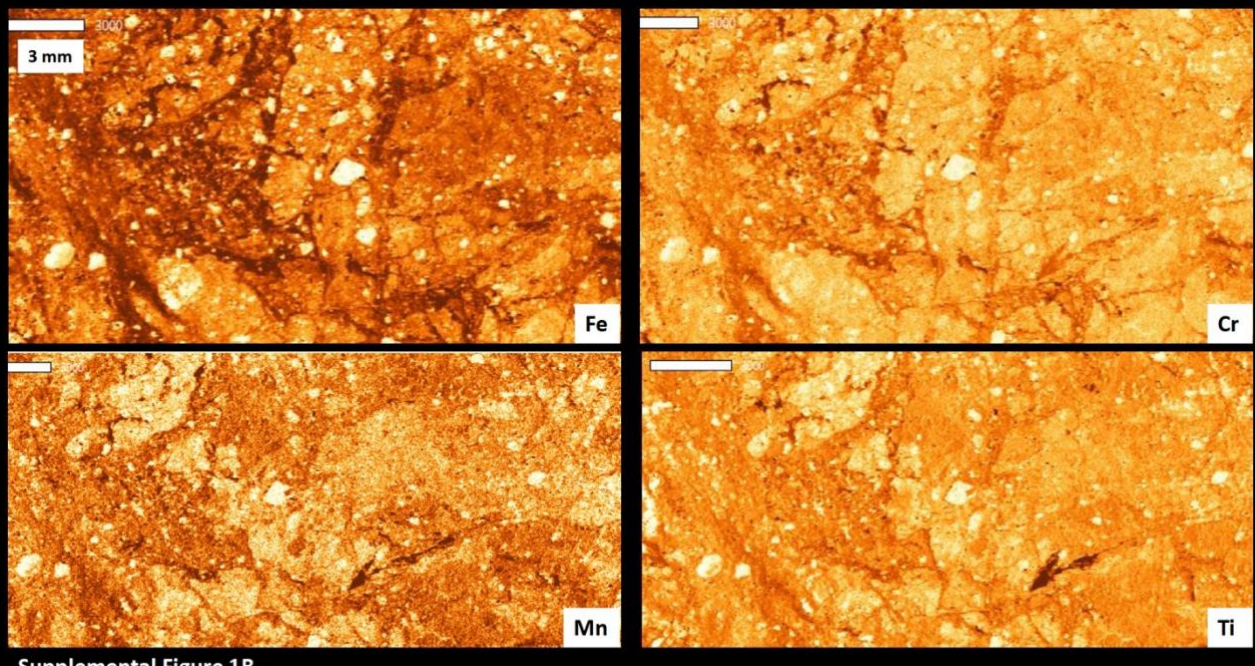

Supplemental Figure 1B.

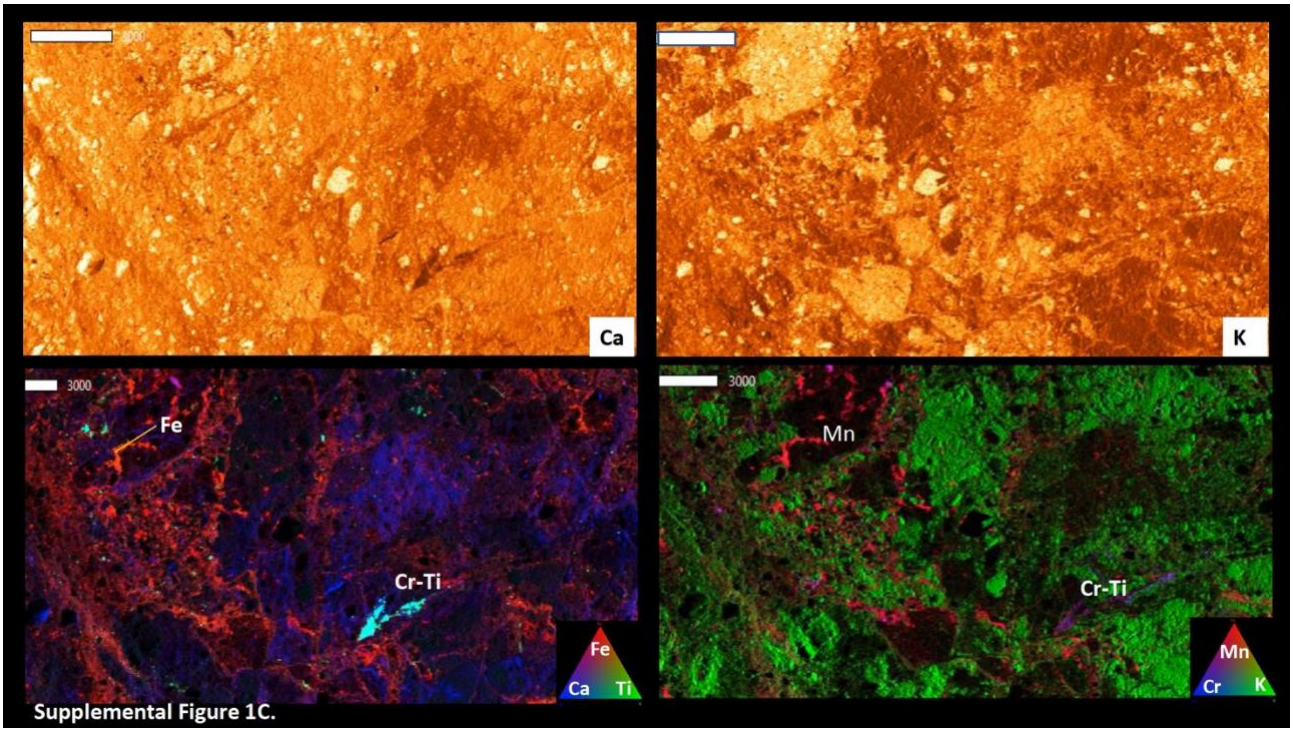

Figure SI-1: XRF maps of a zoomed-in portion of the whole core San Andreas core. The analysis examines the elemental distribution of a part of a damage zone near the Fe-rich fault gouge. **A)** Visible light image of the core showing the location of the image. Fractured and altered rocks encompass a thin slip surface (ss), cataclasite (cata), and Fe-rich gouge (g). Rocks to the left of the slip zone are barely cohesive gouge/pulverized rocks, and the damage zone rocks to the right are moderately indurated. **B)** The shear zone is enriched in Fe, Mn, Cr, and Ti on the left side of the image and in zones with sharp boundaries that cut into the highly damaged rocks. **C)** Elemental maps of Ca and K, and tricolor maps of Fe-Ca-Ti and Mn-Ca-K. The metals-rich zones surround K- and Ca-rich regions that appear to be zones of earlier-formed cataclasites with sharp, straight boundaries. Thin zones have concentrations of Cr and Ti (Cr-Ti). In some places, iron and manganese fill fractures in the earlier cataclasite fragment (Fe).

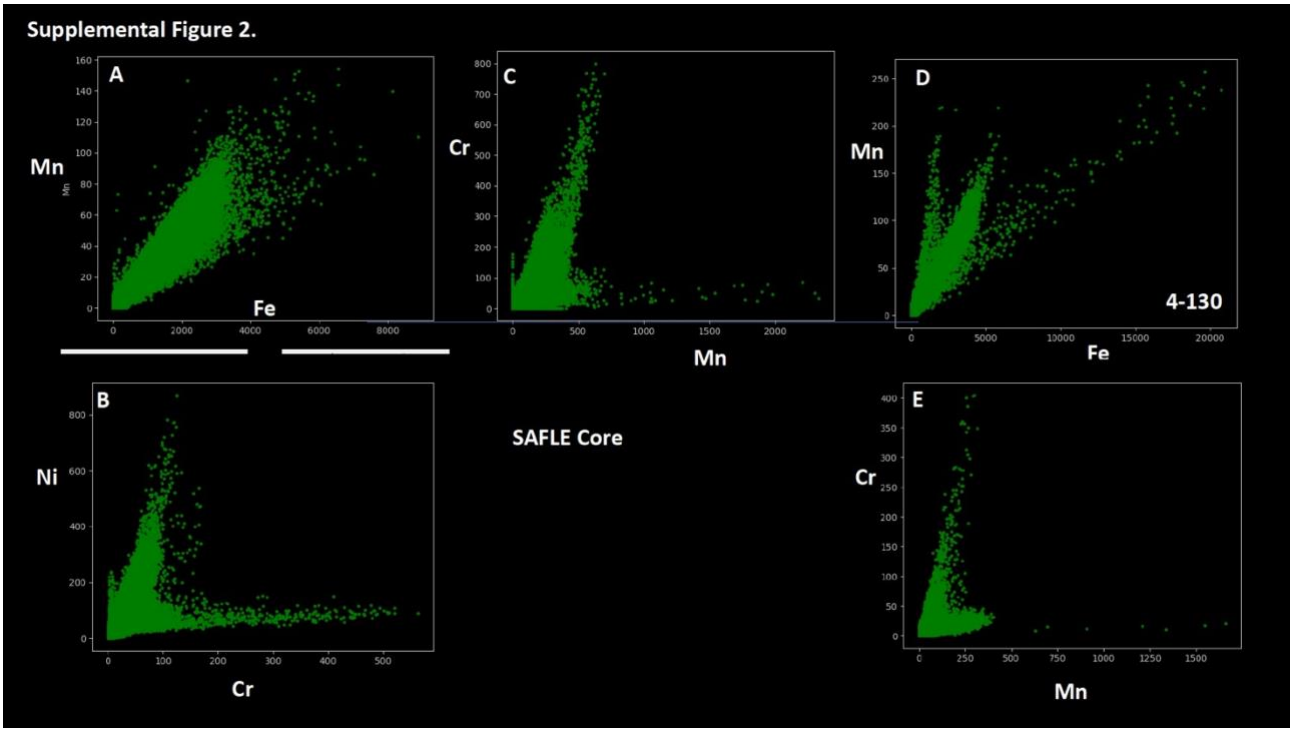

Figure SI-2: Cross-plots among the transition elements for the San Andreas core sample analyses. **A)** Mn-Fe, **B)** Ni-Cr, and **C)** Cr-Mn are used for part of the SAF large core sample, as shown in Supplemental Figure 1. **D and E** Correlation plots for sample – 4-130. For Mn-Fe and Cr-Mn.

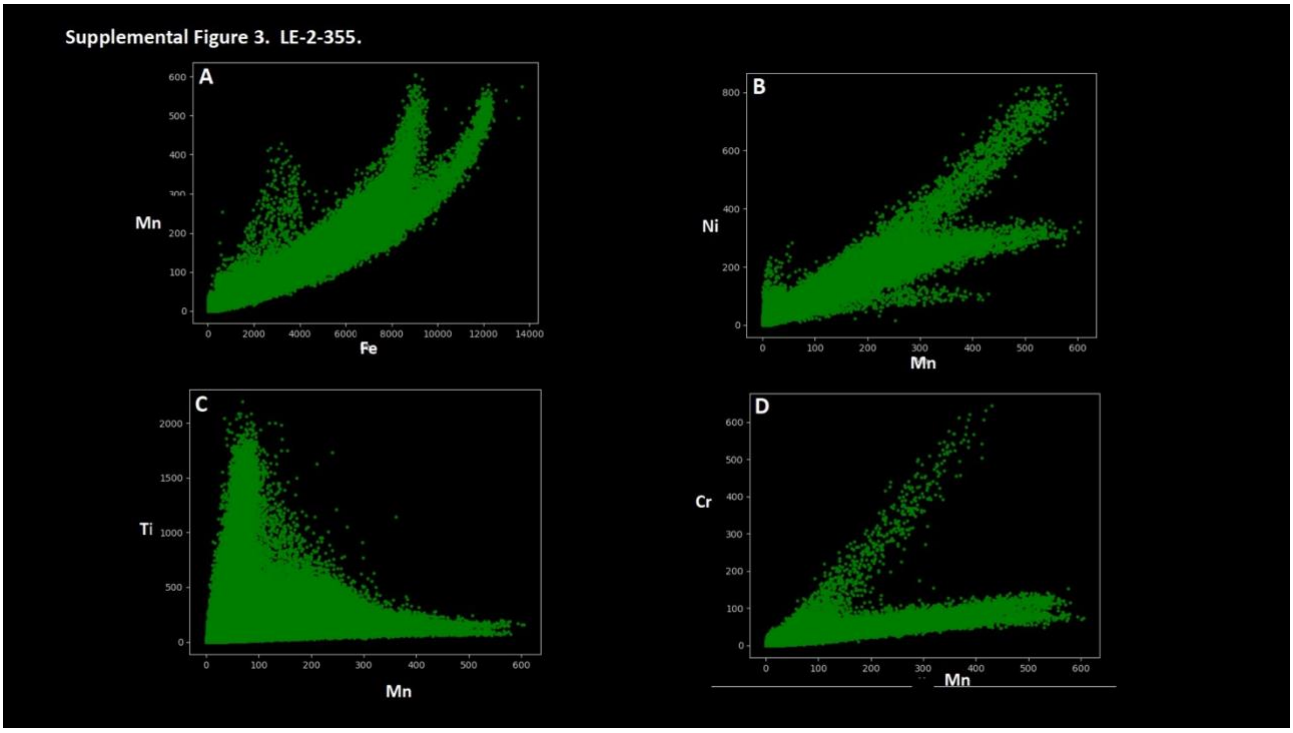

Figure SI-3: Cross-plots among the transition elements for the SAF thin-section sample analyses for sample LE 2-355. **A)** Mn-Fe **B)** Ni-Mn, **C)** Ti-Mn, and **D)** Cr-Mn.

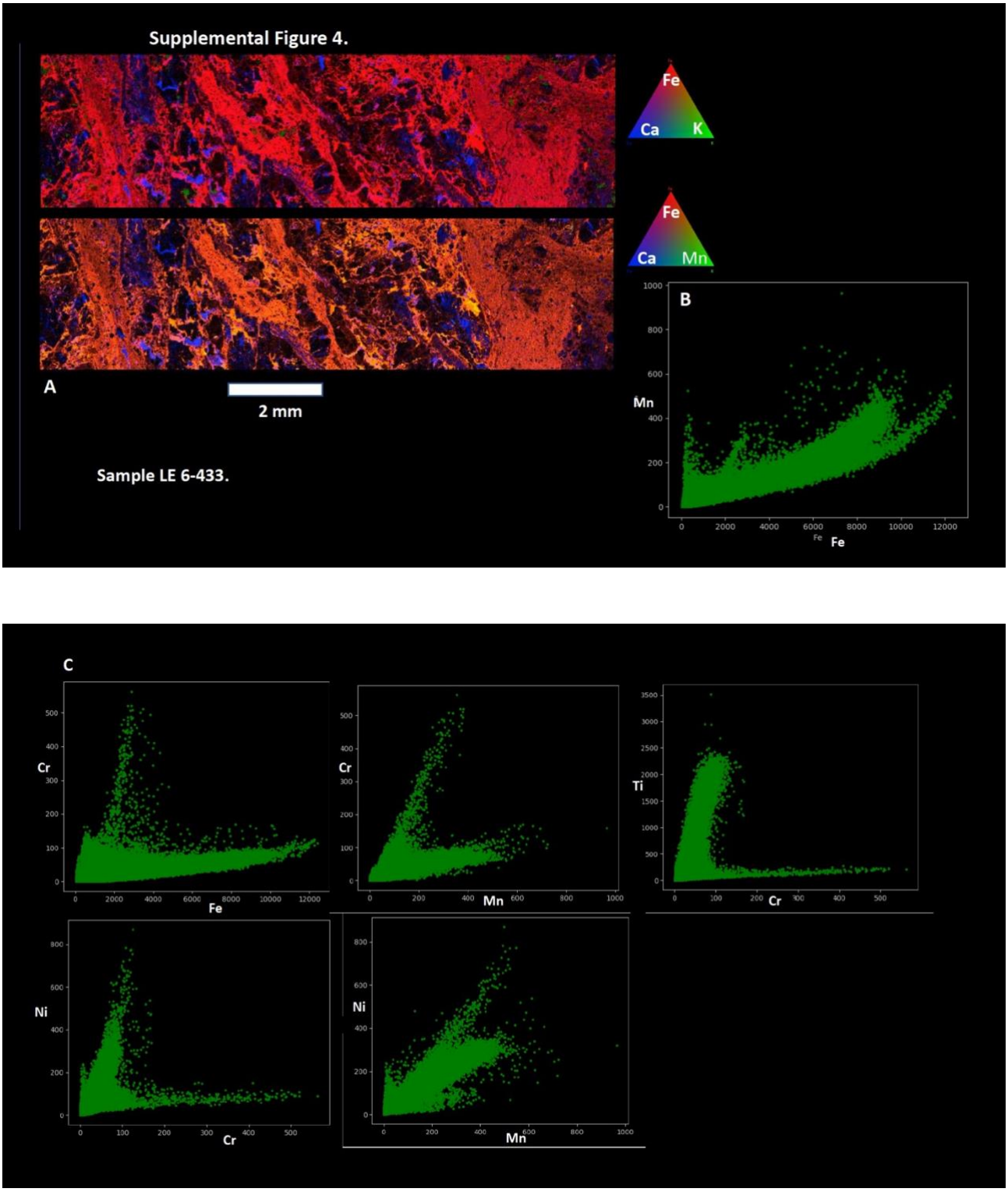

Figure SI-4: Elemental maps and correlation plots for sample 6-433. A) Fe-Ca-K and Fe-Ca-Mn high-magnification tricolor maps of highly sheared Fe-rich zones that cut protolith grains with Ca (probably showing the presence of calcite). **B)** Cross-plot of iron and manganese in the mapped area. **C)** Correlation plots of Cr-Fe, Cr-Mn, Ti-Cr, Ni-Cr, and Ni-Mn in the mapped area of Figure A.